Archives of Hydro-Engineering and Environmental Mechanics
Vol. 57 (2010), No. 1, pp. 43–59
© IBW PAN, ISSN 1231–3726

Gravity- and Turbulence-Dominated Sediment Motion in the Clear-Water Scour Process at a Vertical-Wall Abutment in Pressurized Flow

Alessio Radice[1], Francesco Ballio, Chau K. Tran

Alessio Radice, Politecnico di Milano, Piazza Leonardo da Vinci, 32, 20133 Milano, Italy,
e-mails: alessio.radice@polimi.it, francesco.ballio@polimi.it, chau.tran@mail.polimi.it

(Received October 12, 2009; revised December 03, 2009)

Abstract

Results on the motion of sediment particles on the bottom of the erosion hole are shown for a clear-water scour experiment with a vertical-wall abutment. The paper presents an investigation of particle kinematics starting from the division of the grain instantaneous movements into two populations, namely the "turbulence-dominated" events (those in which the particle motion is triggered by the turbulent flow field) and the "gravity-dominated" events (those in which the particles slide along the slopes of the scour hole due to geotechnical instability). Attention is focused on the well developed stages of the erosion process. For such experimental times, the action of the principal vortex system is particularly evident because the latter is not much stretched along the direction of the mean flow deviation, thanks to the increased flowing area. At the same time, the temporal unsteadiness of the vortices lets a bimodal behaviour of the sediments to emerge. A relevant difference has been found between the dynamics of gravity-dominated and turbulence-dominated events. In addition, it was found that the presence of geotechnical effects in the erosion hole may significantly alter the scour rate. Potential implications of the present results for the modelling of local scour processes are described.

Key words: abutment scour, sediment kinematics, turbulence, sliding

1. Introduction

Local pier and abutment scour is a crucial topic in hydraulic engineering due to the significant social and economical impact of bridge failure. Some case studies are documented, for example by Melville and Coleman (2000), who also demonstrate the high cost of bridge repair or reconstruction. Therefore, reliable tools for scour prediction are necessary for both design and vulnerability evaluation of the structures.

[1] Corresponding author.

Experimental measurement and numerical modelling of the scouring flow field clearly show the horseshoe vortex and the principal vortex as the most evident features of the flow pattern at piers and abutments, respectively (e.g. Dargahi 1989, Kwan and Melville 1994, Dey and Barbhuiya 2005, Nagata et al 2005, Kirkil et al 2008). The vortex structure typically presents a high turbulence level compared to that of the incoming flow: for example, Graf and Istiarto (2002) measured high levels of turbulent kinetic energy upstream of a cylindrical pier, finding that it was also increasing towards the bed; a similar result was found by Dey and Barbhuiya (2005) who measured the turbulent kinetic energy around a vertical-wall abutment on a flat bed and within a scour hole, finding that it was larger in the second case; a significant turbulence level in the flow field within the scour hole was also highlighted by the Large Eddy Simulation (LES) model by Kirkil et al (2008). The presence of external turbulence is believed to cause the possible underestimation of the erosion depth that is typically obtained through numerical models using sediment transport equations based on the time-averaged values (e.g. Nagata et al 2005, Roulund et al 2005). The role of turbulence was also acknowledged by Sumer (2007) who suggested exploring the effect of external turbulence on bridge scour processes as a major route to be taken by future research, since presently no specific tools are available.

Temporal fluctuations in water velocity make the coherent vortical structures unstable in time. For example, Dargahi (1989) showed that the horseshoe vortex upstream of a cylinder in flat bed could not be persistently observed. The temporal variability of the vortex system was also detected by the LES model of Koken and Constantinescu (2008). The distributions of velocity values in junction flows often present a bimodal shape (e.g. Devenport and Simpson 1990, Kirkil et al 2008), indicating that two types of event are usually occurring in the vicinity of the obstacles. The kinematics of the bottom grains clearly reflects the flow pattern. Indeed, a succession of opposite motion events can also be detected, considering the sediment motion at a certain location within the erosion hole. This was demonstrated by the experimental measurements made by Radice et al (2008) and Radice (2009a) for rectangular and trapezoidal abutments, respectively. In these studies, motion events directed towards the obstacles and away from them were recognized in the developed stages of the process. Radice et al (2008) associated the events of sediment motion away from the abutment to sediment pickup and transport by the turbulent flow field, whilst those with motion towards the abutment were associated to sediment sliding. On a qualitative basis the presence of geotechnical effects is relatively well acknowledged: for example, Melville and Raudkivi (1977) described the sediments collapsing irregularly in sand avalanches and suggested that the scour process in evolved condition result from the combination of temporal mean shear stress, weight component (we should highlight here that the sediment weight is both the resisting force for particle pickup and the driving force for geotechnical sliding)

and turbulent agitation. As a matter of fact, Roulund et al (2005) incorporated sediment sliding in their numerical model for local scour at a circular pier.

A quantitative definition of the relevance of sliding for the sediment kinematics in a local scour process is still lacking. Therefore, the purpose of the present paper is to make a specific analysis of event separation, aimed towards a quantification of the relevance of sediment sliding for proper process modelling.

2. Background

The experiment outlined in this paper was performed by Radice et al (2009b) at the Hydraulic Engineering Laboratory of the Politecnico di Milano, Italy. The experiment was run using a rectangular pressure duct having a cross section of 40×16 cm^2. Plastic cylinders with a characteristic size $D = 0.36$ mm and a density of 1.43 kg/dm^3 were used. The water discharge was equal to 18.5 l/s, which corresponded to incipient motion conditions for the sediments in the unobstructed part of the duct. A vertical plate with a length of 10 cm was used as the abutment. Radice et al (2009b) compared the measured temporal trend of the erosion depth to that measured in an earlier experiment with a free surface, obtaining that flow pressurization did not significantly alter the dynamics of scour increase with time. The analysis presented in this paper, however, would not suffer from any possible distortion due to flow pressurization. A reference system is used throughout the manuscript with the x axis aligned with the bulk flow and the y axis oriented leftwards. The coordinates of the upstream nose of the abutment are $x = 100$ cm and $y = 30$ cm. The components of the sediment velocity along the x and y axes are u and v, respectively.

Figure 1 presents the temporal development of the erosion depth, which was measured at the upstream nose of the obstacle ($x = 99$ cm, $y = 30$ cm) and at the junction between the duct wall and the upstream face of the abutment ($x = 99$ cm, $y = 40$ cm). The erosion depths at the abutment nose and at the junction point were measured by means of a laser triangulation sensor and of a ruler attached to the lateral wall, respectively. Consistently with the typical description of the process, the maximum scour is initially located near the abutment nose and it later migrates towards the lateral wall, where it finally remains permanently. The temporal rise of the erosion depth is logarithmic, with the scour rate being largest in the initial stage of the process and progressively lowering. As said in the Introduction, the bimodal nature of the sediment motion events is most evident for the developed stages of the process, where the scour rate is low. Therefore, the following analysis will be focused on an experimental time as large as $T = 2$h 45' (= 9900 s), for which a three-dimensional survey of the geometry of the erosion hole is available. The time under consideration is highlighted in the plot. The survey of the scour hole topography was made using the same laser sensor used for the measurement of the scour depth evolution at the abutment nose. The survey time was approximately

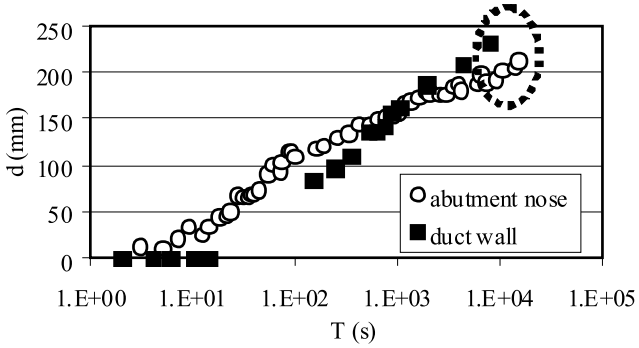

Fig. 1. Temporal development of the scour depth d during the experimental test. The time used for the analysis is highlighted

1 h, during which the experiment was stopped, lowering the water discharge until sediment motion ceased.

During the experiment, Radice et al (2009b) filmed the sediment motion using a black and white CCD camera. Afterwards, the sediment kinematics was measured using the methodology devised by Radice et al (2006), which enables a Eulerian measurement to be made of the concentration C and vector velocity V of the moving particles. Both quantities are defined and measured over a reference area A of the bed. Sediment concentration is defined as $C = W/(A \times D)$, where W is the volume of moving sediments. Sediment concentration was measured using a technique based on image subtraction and filtering of the difference images. Sediment velocity was measured by Particle Image Velocimetry. The solid discharge per unit width is then defined as $q_s = C \times V \times D$, in analogy with earlier literature definitions (e.g. Fernandez Luque and Van Beek 1976, Niño and Garcìa, Parker et al 2003). The focus area relative to the experimental time considered here is depicted in Figure 2(a), where also the cells with $A = 2 \times 2$ cm^2 used for the Eulerian measurement are shown. The films taken by Radice et al (2009b) had a duration of 20 s, due to limited possibility of image storage in the RAM of the PC used. On the other hand, Radice et al (2009b) showed that data from some successive sequences can be averaged together, provided that the averaging period is much smaller than the characteristic time scales associated with process development. In other words, the variation of the maximum erosion depth within the period considered for averaging must be a negligible fraction of the scour level previously achieved. Figure 2(b) presents the sediment motion pattern obtained by averaging data from eleven movies, to which the time period from 8960 to 11960 s corresponded (total film time is obviously 220 s; the period of 3000 s results from time intervals needed for saving the video onto the PC). Radice et al (2009b) interpreted the upstream direction of the sediment motion as a footprint of the principal vortex system, and used results similar to that presented here to hypothesize that the principal vortex is compound of at least two

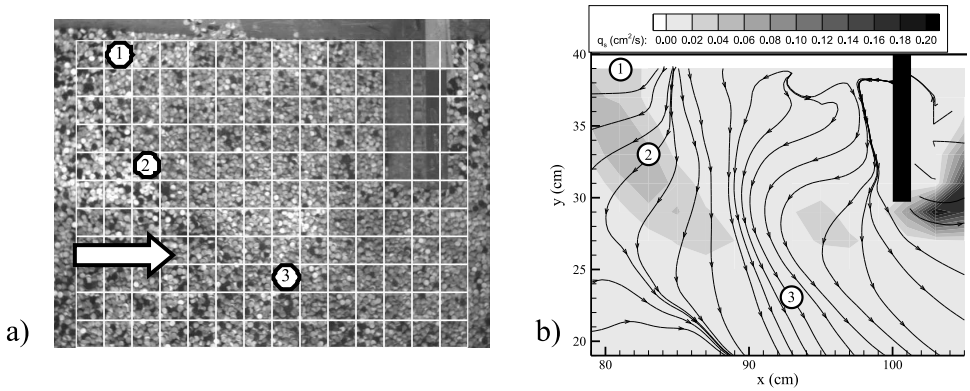

Fig. 2. a) map of the measuring grid over a picture of the scour hole (bulk flow direction indicated); b) time-averaged sediment motion pattern (greyscale contour levels of time-averaged solid discharge per unit width and sediment motion lines; locations used for the plots in Figure 3 are indicated). In both pictures flow direction is rightwards

vortices with horizontal axis (one located around $x = 95$ cm, $y = 30$ cm and the other around $x = 83$ cm, $y = 30$ cm).

Radice et al (2008) showed that the instantaneous direction of the moving sediments can be significantly different from the time-averaged one. In particular, Radice et al (2008) showed that, at some locations, movements departing from the abutment and directed towards it continuously alternated. The authors hypothesized that the double behaviour is due to succession of scouring by the principal vortex and sediment sliding, and that it is weaker where the principal vortex system is stretched along the main flow direction. Figure 3 (the reader should now ignore the circular sector, whose meaning shall be explained in the following sections) presents some sample polar plots of grain velocity, in which each marker represents an instantaneous velocity value measured within the observation period. The plots are consistent with the earlier findings: for example, considering position (1), which is upstream of the abutment and near the lateral wall of the duct (see Figure 2), movements with $u < 0$ (consistent with the expected structure of the principal vortex) and $u > 0$ (consistent with geotechnical effect) can be observed. The transverse motion at position 1 is inhibited by proximity to the lateral wall. It is reasonable to expect a flow structure with small lateral velocity at that location. As a result, the sediment transverse motion is also small and, on average, vanishing. Opposite movements are also evident for position (2), which is again upstream of the obstacle. On the contrary, the double behaviour is not apparent for position (3), which is on the abutment side.

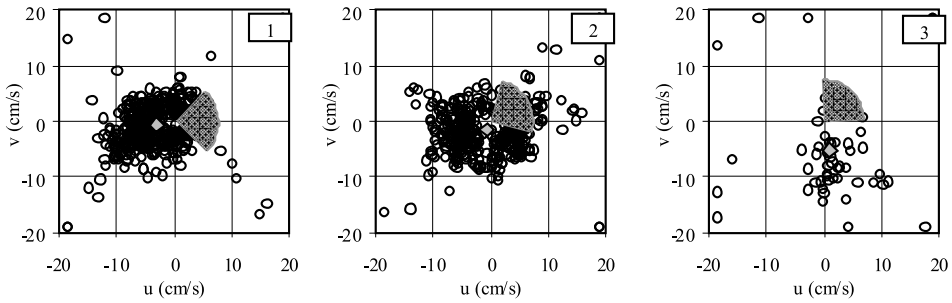

Fig. 3. Sample polar plots with indication of the boundary for selection of the "gravity-dominated" motion events. The grey diamond corresponds to average velocity (all events). Location numbers correspond to those in Figure 2

3. Method of Analysis

The key object of the following analysis is the identification of the motion events that can be associated with sediment sliding along the slopes of the erosion hole. We shall now point out that, in our opinion, it is hardly possible for a motion event to be entirely due to geotechnical effects, with no role of the flow field. Therefore, in the following we will use the expression "gravity-dominated event" instead of "sliding event" to identify an event with a major role in the geotechnical component. In the same way, we will use the term "turbulence-dominated" to identify the other events. This section describes the method used to automatically label a motion event as "gravity-dominated".

Figure 4(a) depicts the three-dimensional surface identifying the geometry of the erosion hole obtained from the survey. Furthermore, Figure 4(b) presents the contour lines of bed elevation and the corresponding gradient map highlighting the local directions and intensities of maximum slope.

We define a gravity-dominated event as one satisfying two conditions, namely: (i) the direction of sediment motion and that of maximum slope delimit an angle whose amplitude does not exceed $\pi/4$ (in absolute value); (ii) the velocity of the motion event is smaller than a threshold determined considering the ideal frictionless falling of a mass along a submerged inclined plane; in such condition, we assume that the effective acceleration responsible for mass falling is $g\times\sin\beta$, with g and β being the acceleration due to gravity and the slope of the inclined plane, respectively. In our ideal picture we determine the maximum velocity of a gravity-dominated event w as the fall velocity with reduced gravity:

$$w = \sqrt{\frac{\frac{4}{3} g \sin\beta \, D \, (s-1)}{\frac{24\mu}{\rho w D} + 1.5}}, \tag{1}$$

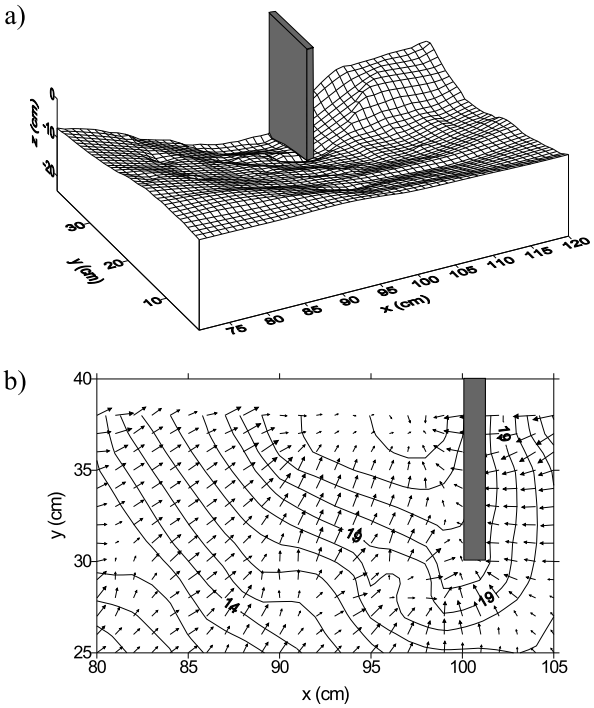

Fig. 4. a) bed topography in the scour hole, where z is the vertical upwards coordinate and $z = 0$ corresponds to the original bed level; b) contour lines of the scour depth d and gradient map of the deepest part of the scour hole. In both pictures the abutment is indicated in grey. Data not available for $y > 38.5$ cm

with the following symbol meaning: $s = \rho_g/\rho$, with ρ_g and ρ as the densities of particles and water, respectively, μ = dynamic viscosity of water. In the above expression, the equation for the drag coefficient on the particle given by Chanson (1999) was used. It is acknowledged that the threshold for sediment velocity is presumably overestimated, since we do not account for of any effect due to sediment roughness; furthermore, the threshold is based on the asymptotic sliding velocity and does not account for any acceleration of the particles. In synthesis, the boundary for the identification of a gravity-dominated event in a polar plot is a circular sector (as those shown in Figure 3 for the sample locations considered).

4. Results

4.1. Statistical Distributions of Particle Velocity and Direction

We present the results of a statistical analysis of particle velocity and direction, in terms of the probability density function (pdf) and of the Cumulative Frequency Distribution (CFD). The distributions were computed with reference to all the data samples for all the measuring locations upstream of the abutment (for a total cell

number of 121) and are depicted in Figure 5. It should be pointed out here that a zero angle corresponds to a movement in the direction of the local gradient of the erosion hole that angles are positive if counter-clockwise. The distributions for gravity-dominated (*GD*) and turbulence-dominated (*TD*) events have been normalized, so that the sum of the areas of the two distributions equals the area of the pdf for all events (*ALL*). An overlap between the typical velocities for *GD* and *TD* events can be detected from Figure 5(a), which is a consequence of low-velocity events for the *TD* motion outside of the particle direction range for *GD* motion. The CFD of particle velocity (Figure 5b) shows that 40% of the *TD* events have a velocity lower than the threshold for identification of a *GD* event. The pdf of sediment velocity for *GD* events presents an abrupt descent as the threshold is approached, consistent with our approach involving a sharp distinction of events while the transition between the two populations is relatively gradual. The pdf of particle direction for the *TD* events shows that the most frequent angle is around $\pm\pi$ that, given the relative reference used, is opposite to the direction of maximum slope in the erosion hole. This is consistent with the expected structure of the principal vortex, having radial direction in the hole. On the contrary, and consistently with the criterion for recognition, the pdf of direction for the *GD* events is bounded between $\pm\pi/4$ and presents a peak for zero angle. As a result, the pdf of direction for all the events presents (consistently with the earlier literature referenced above) a bimodal shape, with a mode aligned with the gradient and the other opposite to it.

4.2. Relationship between the Statistical Moments of the Quantities

Sediment motion physics can be analyzed through observation of the relationships between the concentration and velocity of the moving sediments and the resulting solid discharge, as successfully proved by Ballio and Radice (2007) and Radice and Ballio (2008) for one-dimensional bed load over a plain bed and by Radice et al (2009b) for scour at a vertical-wall abutment. In the cited works, a different role of sediment concentration and velocity in determining the resulting sediment transport rate was demonstrated. In this paper, we hypothesize that the dynamics of the sediment transport process is different for the different event classes and thus we have repeated the correlation analysis of Radice et al (2009b) having preliminarily divided the sediment motion data into some populations based on event recognition. The event distinction is presented in Figure 6, where the *GD* events lie within the grey sector and the *TD* events lie in the remaining part of the plot. Sub-parts of the *TD* domain can be further obtained considering the turbulence-dominated events with a velocity lower than the threshold for ideal sliding (*TDV*, region bounded by the thin dotted line) and the turbulence-dominated events with a direction comparable to that for gravity-dominated motion (*TDD*, region bounded by the thick dash-dotted line). In the following, we will which refer again to statistics of the

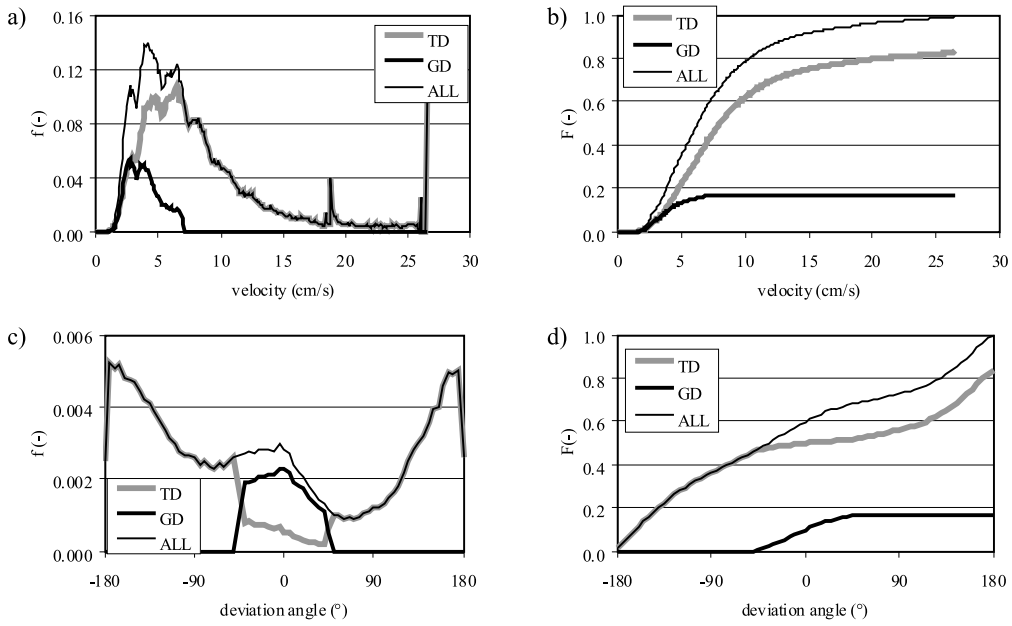

Fig. 5. a) probability density function of particle velocity; b) Cumulative Frequency Distribution of particle velocity; c) probability density function of particle direction compared to the gradient of the erosion hole; d) Cumulative Frequency Distribution of particle direction compared to the gradient of the erosion hole

global sample, which have been previously indicated with *ALL*. A remark has to be made with reference to the intermittent nature of the sediment transport process. The analysis of Radice et al (2009b) has shown that the intermittency of sediment motion is relevant in local scour, that is, at a certain location the sediments do not move continuously within the observation period whilst some stillness terms are present. It is evident that the no-motion events are excluded from the analysis presented in this paper, which instead refers only to the instants with actual particle movement.

The relationship between the first order statistics of the quantities is depicted in Figure 7, where each marker corresponds to a measuring location within the erosion hole. The lower bound of the concentration is evident in Figures 7(a) and 7(b), as that quantity is limited by the value corresponding to a single moving particle. The inclined upper boundary of the point cloud in Figure 7(c) is a reflection of this behaviour. The relationship between concentration and velocity (Figure 7a) highlights the separation between the *GD* and *TD* events. This is, to a certain extent, obvious, since the distinction between *GD* and *TD* has been made on the basis of a velocity threshold, yet it should be borne in mind that labelling an event as *GD* also requires satisfaction of a condition on velocity direction. If we consider

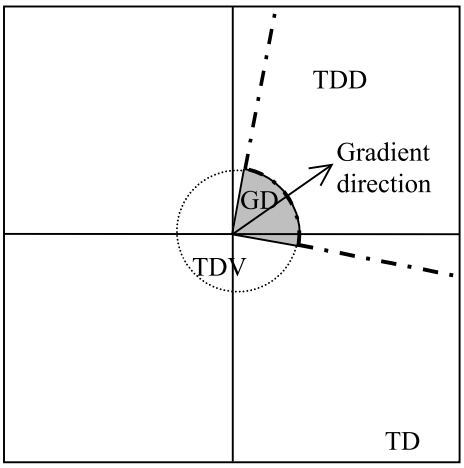

Fig. 6. Distinction between the sediment motion events in a polar plot of sediment velocity. Codes: GD, gravity-dominated; TD, turbulence-dominated; TDD, turbulence-dominated with a direction within the threshold for GD; TDV, turbulence-dominated with a velocity lower than the threshold for GD. TD comprises TDD, TDV and the external region

the comparison between the *GD* and *TDV* events (which are in this way bounded by the same velocity value), we can still see that *TDV* events are characterized by average velocities slightly larger that those for the *GD* events, indicating that typical velocities in turbulence-dominated event are larger than the corresponding ones for gravity-dominated events. This shall be even more evident if we remember that the threshold velocity used for identification of sediment sliding is an overestimation based on ideal frictionless sliding. Sediment concentration range is instead similar for *GD* and *TDV*. The analogy in the concentration range may be interpreted assuming that *GD* events be not triggered by gravity alone, but, due for example to sediment packing, a certain force exerted by the flow field is needed to activate sediment sliding along the slopes of the erosion hole. If we assume that the footprint of a turbulent events has a certain size, then the concentration of motion will be similar for *TD* and *GD*. Finally, looking at the points for *TDD* in Figure 7(a), we see that the points for low concentration are more dense than those for high concentration, indicating that a motion towards the bottom of the erosion hole triggered by turbulence is typically moving few particles at a relatively high velocity.

4.3. Relevance of Gravity-Dominated Events in the Scour Process

In the precedent sub-section the different dynamics of *GD* events compared to that of the *TD* events has been demonstrated. While this is interesting from the point of view of the physical processes involved, it is not ascertained yet whether or not gravity can significantly alter the scour development. A first index of the relevance

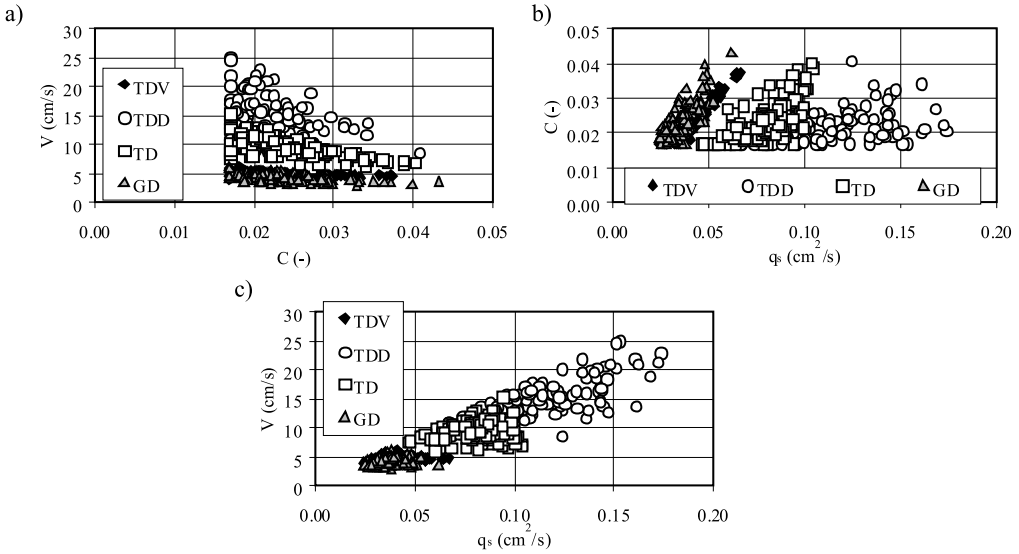

Fig. 7. Relationship between the time-averaged solid discharge per unit width, sediment concentration and sediment velocity for the different event classes. See Figure 6 for legend meaning

of gravity can be obtained considering the percentage of *GD* events over all the motion events at a single location. The relationship between such percentage and the slope of the scour hole is depicted in Figure 8, where, again, each marker corresponds to a location in the erosion hole. The percentage of *GD* events does not appear to be correlated with the local slope of the hole (indicating that the dynamics of turbulence highly complicates the relationship between gravity and motion). Most values are lower than 40%, with some isolated ones up to 70%. This, however, is still not enough to prove or confute the relevance of gravity, because the relative importance of this effect should be analyzed in terms of the resulting solid discharge.

We assume the average sediment motion at a certain location to be the result of the composition between two major driving effects, namely turbulence and gravity. Therefore, the sample of the instantaneous quantities measured at each location has been divided into the *GD* and *TD* sub-samples, with the purpose to compare the two average values representative of the two sub-samples. The comparison is depicted in Figure 9. The sediment concentration (Figure 9a) is similar for the two event types, as expectable given the above considerations. For sediment velocity (and then for solid discharge) a preliminary consideration has to be made about the quantities to be compared. As pointed out by Radice et al (2009a) the instantaneous magnitude of sediment velocity and solid discharge is computed through a non-linear combination of the components along the coordinate axes; the time-averaged value (for example

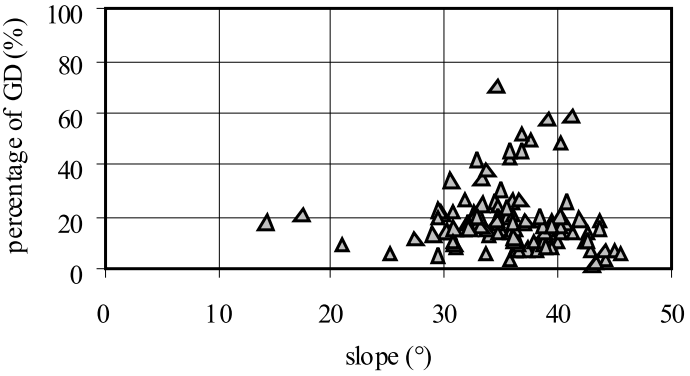

Fig. 8. Relationship between slope of the erosion hole and percentage of gravity-dominated events

for velocity) can be computed in two ways (that will be indicated with different subscripts):

$$V_1 = \frac{1}{N}\sum_{i=1}^{N}\sqrt{u_i^2 + v_i^2}; \tag{2}$$

$$V_2 = \sqrt{\left(\frac{1}{N}\sum_{i=1}^{N} u_i\right)^2 + \left(\frac{1}{N}\sum_{i=1}^{N} v_i\right)^2}. \tag{3}$$

In Equations (2) and (3), u and v are the instantaneous velocity components along the x and y axes, as previously defined, and N is the sample size. The V_1 average is an indicator of the process dynamics and of the typical strength of the driving agent. By contrast, the scouring trend is related to the sediment continuity equation over a certain time period. Such equation involves the time-averaged components of sediment velocity (through a divergence operator, as shown below), which are related to V_2. Precedent analyses were referred to the physics of sediment motion and, consistently with that, were focused on V_1 (and on the analogous average for the sediment transport rate). In this sub-section we are concerned with the erosive pattern and therefore the key quantity to which we will refer is V_2 (and the analogous average for the solid discharge). The comparisons are set out in Figures 9(b) to 9(e). It is evident that, as expectable, both velocity and solid discharge are much larger for *TD* than for *GD* as long the "1" averages are computed, whilst the properties become more similar if we compute the "2" averages. The result of the analysis is that the *GD* events may be able to induce a solid discharge comparable to that for the *TD* events, thanks to the direction of *GD* events being always similar whereas that of the *TD* ones is much more dispersed.

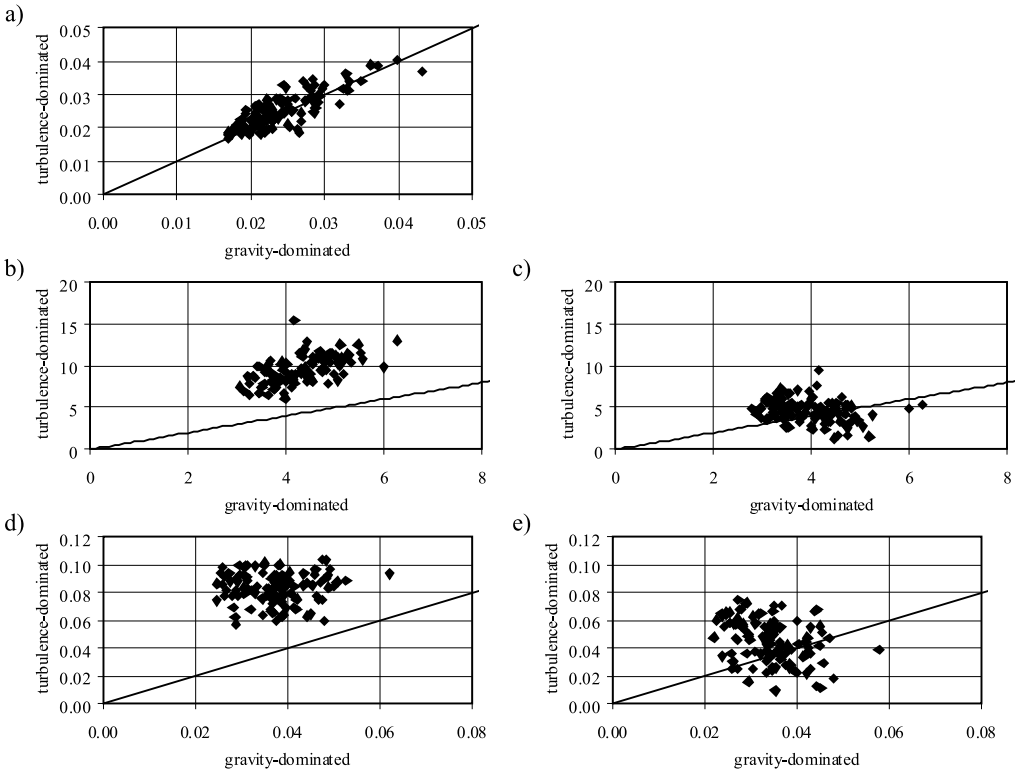

Fig. 9. Comparison between: a) sediment concentration, b) sediment velocity (cm/s) averaged with (2), c) sediment velocity (cm/s) averaged with (3), d) solid discharge (cm^2/s) averaged like (2), e) solid discharge (cm^2/s) averaged like (3), for *GD* and *TD* motion events

Another evaluation of the role of *GD* events is set out in Figure 10. In each plot, we present the contour lines (dashed, some values indicated) of the erosion depth, the gradient map of the erosion hole (arrows), the sediment motion lines (continuous line) and the sediment transport rate computed as the "2" average (greyscale contour lines). The time-averaged sediment motion pattern is computed for *GD* events in Figure 10(a), for *TD* events in Figure 10(b) and for all the events (that is, depicting the actual resulting sediment motion pattern) in Figure 10(c). The sediment motion lines for *GD* are obviously consistent with the gradient map, given the threshold on velocity direction for identification of a *GD* event. Furthermore, the sediment motion lines for the *TD* events and for the entire population are not much different, indicating that *GD* events do not affect much the general sediment direction. On the other hand, the total-averaged solid discharge is lower than the *TD*-averaged, due to the action of *GD* events. For example, maximum solid discharge of *TD* events (Figure 10b) equals 0.075 cm^2/s for the location x = 89 cm, y = 23 cm; corresponding solid discharge for *ALL* events is 0.062 cm^2/s, with a significant reduction. As a consequence, the erosion pattern resulting from the data in Figure

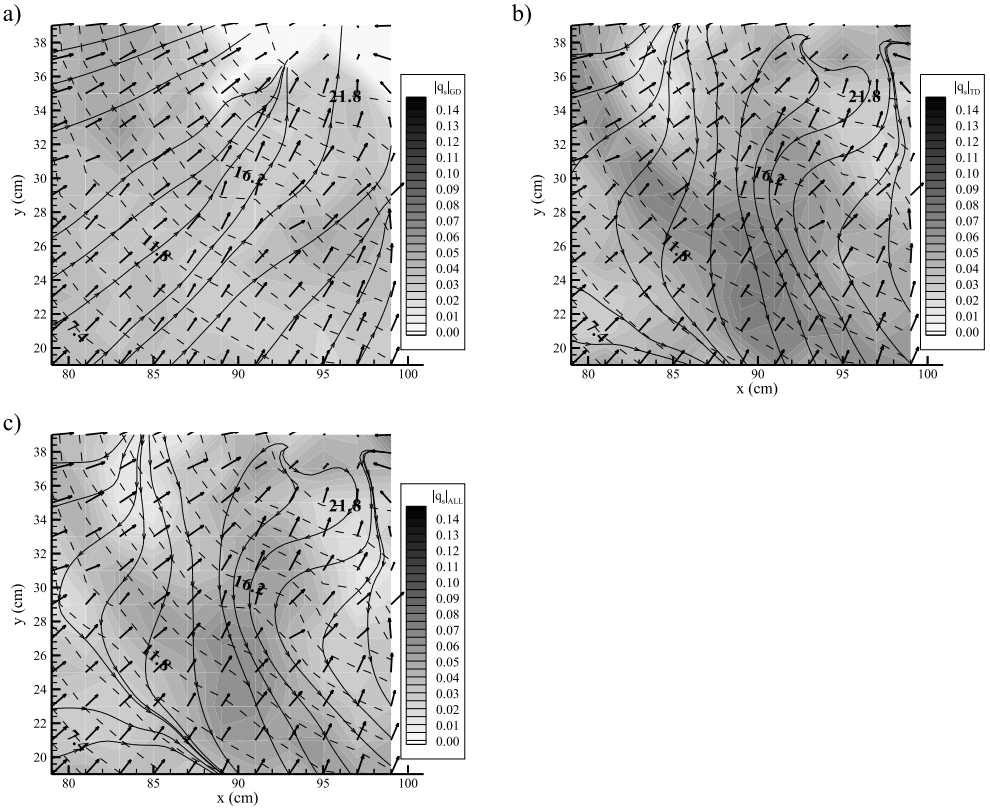

Fig. 10. Average sediment motion pattern for different events (*GD*, *TD* and *ALL*). Geometry of the erosion hole (dashed contour lines, gradient map) superimposed

10(b) will be different from that obtained from the data in Figure 10(c). We have computed a scour rate as:

$$\dot{d} = \frac{\nabla \cdot \mathbf{q_s}}{1-p}, \tag{4}$$

where d is the local scour depth and p is porosity, assumed to be equal to 0.5. This value is larger than the typical ones, but we should consider that the sediments moving are not as packed as in a layer of still particles. However, it is only a constant that does not affect the resulting considerations. The map of the erosion trend is depicted in Figure 11 for the three types of events. If we compute the average over all the locations as a global indicator of the scour rate, we find the latter being 0.0044 cm/s for the *TD* map and 0.0024 cm/s for the *ALL* map, indicating that the estimated scour rate for *TD* events is 1.85 times that for the *ALL* events. It should be remarked here that these scour rates cannot be compared to that obtained from

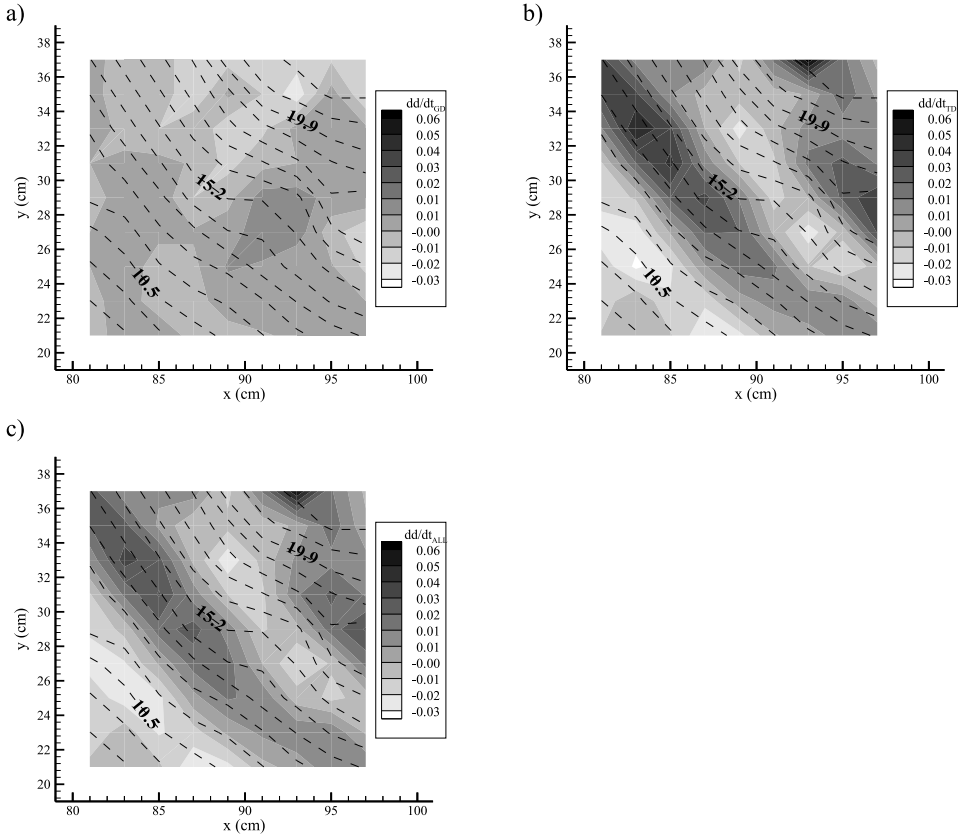

Fig. 11. Average scour rate computed for different events (*GD*, *TD* and *ALL*). Dashed contour lines indicate the erosion depth

the temporal development of the erosion depth, since the actual scour rate depends also on intermittency of sediment motion, that has been discarded in the present analysis.

5. Conclusions

In this work, we have presented a quantitative evaluation of the relevance of geotechnical effects in the clear-water scour process at a vertical-wall abutment. Indeed, it has been previously found in the literature that the principal vortex system is unstable in time and that induces a bimodal behaviour of the sediments on the bottom of the erosion hole. Moreover, attempts to incorporate the effect of sediment sliding in the scour modelling have been proposed. Yet, to the best of our knowledge, no proper data were available for a proper quantification of the role of sliding in bridge scour.

Starting from the measurements of the sediment kinematics taken during an earlier work, we have separated "gravity-dominated" effects and "turbulence-dominated" effects. A clear separation between these two types of events was not apparent. We have decided to recognize the *GD* events based on two criterions, namely (i) a direction of motion similar to the local slope of the scour hole and (ii) a velocity bounded by the maximum ideal velocity of sliding over an inclined plane.

The analysis of the experimental data has led to two major conclusions, namely (i) the dynamics of sediment motion in *GD* events is different from that in *TD* events and (ii) the presence of *GD* events may be able to alter the temporal development of the erosion process in the evolved scour stages. This findings support the need for properly incorporating geotechnical effects in the modelling of local scour processes. On the other hand, a role of local turbulent events of the flow field has been hypothesized for triggering the geotechnical sediment motion; therefore, it is not straightforward to define proper strategies for modelling such effects. The present paper does not aim to provide fresh updates to modelling strategies, but further research will be devoted to gaining extensive data for proper support to modelling.

Acknowledgments

This research was supported by the Italian Ministry of University and Research under the "MOMICS" PRIN Program. The Directorate for Development Cooperation of the Italian Ministry of Foreign Affairs is acknowledged for the doctorate scholarship granted to Tran Kim Chau.

References

Ballio F., Radice A. (2007) Grain kinematics in weak linear transport, *Archives of Hydro-Engineering and Environmental Mechanics*, **54** (3), 223–242.

Chanson H. (1999) *The Hydraulics of Open Channel Flow: an Introduction*, Elsevier Butterworth-Heinemann.

Dargahi B. (1989) The turbulent flow field around a circular cylinder, *Experiment in Fluids*, **8**, 1–12.

Devenport W. J., Simpson R. L. (1990) Time-dependent and time-averaged turbulence structure near the nose of a wing-body junction, *Journal of Fluid Mechanics*, **210**, 23–55.

Dey S., Barbhuiya A. K. (2005) Flow field at a vertical-wall abutment, *Journal of Hydraulic Engineering*, **131** (12), 1126–1135.

Fernandez Luque R., Van Beek R. (1976) Erosion and transport of bed-load sediment, *Journal of Hydraulic Research*, **14**, 127–144.

Graf W. H., Istiarto I. (2002) Flow pattern in the scour hole around a cylinder, *Journal of Hydraulic Research*, **40** (1), 13–20.

Kirkil G., Constantinescu S. G., Ettema R. (2008) Coherent structures in the flow field around a circular cylinder with scour hole, *Journal of Hydraulic Engineering*, **134** (5), 572–587.

Koken M., Constantinescu G. (2008) An investigation of the flow and scour mechanisms around isolated spur dikes in a shallow open channel: 2. Conditions corresponding to the final stages of the erosion and deposition process, *Water Resources Research*, **44**, W08407, doi: 10.1029/2007WR006491.

Kwan R. T. F., Melville B. W. (1994) Local scour and flow measurements at bridge abutments, *Journal of Hydraulic Research*, **32** (5), 661–673.

Melville B. W., Coleman S. E. (2000) *Bridge scour*, Water Resources Publications, LLC, Highlands Ranch, Colorado, USA.

Melville B. W., Raudkivi A. J. (1977) Flow characteristics in local scour at bridge piers, *Journal of Hydraulic Research*, **15** (4), 373–380.

Nagata N., Hosoda T., Nakato T., Muramoto Y. (2005) Three-dimensional numerical model for flow and bed deformation around river hydraulic structures, *Journal of Hydraulic Engineering*, **131** (12), 1074–1087.

Niño Y., Garcìa M. (1994) Gravel saltation: 2. Modeling, *Water Resources Research*, **30**, 1915–1924.

Parker G., Seminara G., Solari L. (2003) Bed load at low Shields stress on arbitrarily sloping beds: Alternative entrainment formulation, *Water Resources Research*, **39**, 1183.

Radice A., Ballio F. (2008) Double-average characteristics of sediment motion in one-dimensional bed load, *Acta Geophysica*, **56** (3), 654–668.

Radice A., Ballio F., Porta G. (2009a) Local scour at a trapezoidal abutment: sediment motion pattern, *Journal of Hydraulic Research*, **47** (2), 250–262, doi: 10.3826/jhr.2009.3356.

Radice A., Malavasi S., Ballio F. (2006) Solid transport measurements through image processing, *Experiments in Fluids*, **41** (5), 721–734, doi: 10.1007/s00348-006-0195-9.

Radice A., Malavasi S., Ballio F. (2008) Sediment kinematics in abutment scour, *Journal of Hydraulic Engineering*, **134** (2), 146–156.

Radice A., Porta G., Franzetti S. (2009b) Analysis of the time-averaged properties of sediment motion in a local scour process, *Water Resources Research*, **54**, W03401, doi: 10.1029/2007WR006754.

Roulund A., Sumer B. M., Fredsøe J., Michelsen J. (2005) Numerical and experimental investigation of flow and scour around a circular pile, *Journal of Fluid Mechanics*, **534**, 351–401.

Sumer B. M. (2007) Mathematical modelling of scour: A review, *Journal of Hydraulic Research*, **45** (6), 723–735.